RECENT CONTRIBUTIONS TO THE SOLUTION OF NONLINEAR AERODYNAMIC INTERFERENCE PROBLEMS

D. Hummel

Institut für Strömungsmechanik
Technische Universität Braunschweig

Germany

1. Introduction

It is well-known, that for attached flow around a large-aspect-ratio wing the lift and pitching-moment coefficients depend linearly on the angle of incidence as shown in Fig.1. In the flow downstream of the wing a trailing vortex sheet is formed, which slightly departs from the wing plane and rolls up in spanwise direction from both sides. For low-aspect-ratio wings on the other hand the flow separates from the leading-edges even at small angles of incidence. A free vortex sheet rolls up to form two concentrated vortices over the upper surface of the wing. Thus, the position of the trailing vortices deviates largely from the wing plane not only far downstream of the wing but also in its vicinity. This leads to the well-known nonlinear dependence of the aerodynamic coefficients of such wings from the angle of incidence as given in Fig.1.

The principle of aerodynamic theory is to find a theoretical representation of the flow, which takes into account the important properties of the real flow and which neglects higher order effects, which have no significant influence on the results and which therefore would complicate the theoretical treatment quite unnecessarily.

In linear theory L. Prandtl [1] in his famous lifting-line theory for large-aspect-ratio wings proposed to neglect friction effects with the exception of the Kutta condition of zero load at the trailing-edge and to assume the trailing vortex sheet to be flat and to be situated in the plane of the wing. This means, that the trailing vortices are fixed with respect to the wing which leads to the linear dependence of the aerodynamic coefficients on the angle of incidence. The excellent agreement between the linear theory based on this flow model and experiments indicates that Prandtls concept retained the essential properties of the flow and that only unimportant effects have been omitted. Wing-fixed trailing vortex sheets are the basis of all linear theories from the well-known lifting-surface theories of H. Multhopp [2] and E. Truckenbrodt [3] for the calculation of local lift and pitching-moment distributions up to the modern panel methods by J.L. Hess, A.M.O. Smith [4], P.E. Rubbert et al. [5], F.A. Woodward [6], R.L. Carmichael [7], Th.E. Labrujere et al. [8] and W. Kraus, P. Sacher [9] for the calculation of the pressure distribution on the wing surface. Wing-fixed trailing vortex sheets are also successfully used for the solution of linear interference problems. Using this concept lift and pitching-moment of wing-body-combinations have been calculated by X. Hafer [10], whereas the pressure distribution on such configurations is given by the panel methods [4] and [6] to [9], mentioned above. As another linear interference problem a large-aspect-ratio wing in ground proximity can also be treated by a slight modification of Prandtls wing-fixed vortex system: The well-known linear dependence of the aerodynamic coefficients on the angle of incidence at large ground distances is well predicted by a linear theory, in which the trailing vortices are assumed to be situated parallel to the ground.

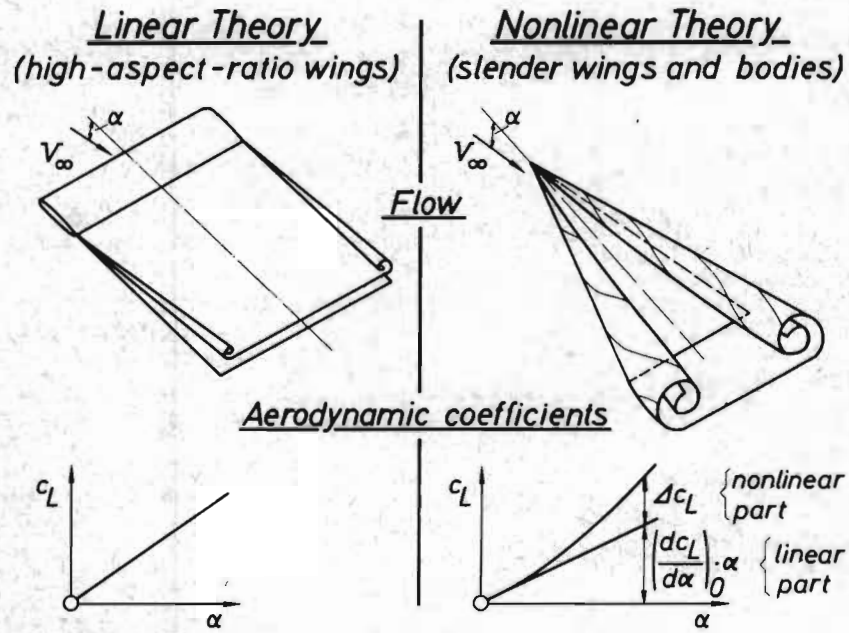

FIGURE 1: Linear and nonlinear theory for wings of different aspect ratios

Methods of this kind are due to F. Thomas [11], U. Ackermann [12], K. Gersten [13] and G.H. Saunders [14].

In nonlinear theory Prandtls vortex model has to be altered in such a way, that the position of the trailing vortices with respect to the wing is a function of the angle of incidence. U. Ackermann [15] and C.H. Fox [16] have shown that a single vortex sheet originating from the trailing edge of the wing and located at a certain angle relative to the wing plane leads only to a very much smaller nonlinear part of the aerodynamic coefficients than experiments show. Therefore, the main nonlinear effect results from the free vortices located over the upper surface of the wing, whereas the position of the trailing vortices far downstream has no significant influence on the nonlinear part of the aerodynamic coefficients. A nonlinear theory for the calculation of the overall forces and moments of slender wings with arbitrarily shaped planform is due to K. Gersten [17]. In this theory a simple vortex model is used the free vortices of which leave the wing surface at an angle of $\varepsilon = \alpha/2 = \text{const}$. Other nonlinear theories aimed at the calculation of the pressure distribution of slender wings and bodies have been developed by C.E. Brown, W.H. Michael [18], K.W. Mangler, J.H.B. Smith [19], J.H.B. Smith [20] and E.S. Levinsky, M.H.Y. Wei [21] by means of vortex models more closely related to the physical flow, but these theories are restricted to slender conical wings. More recently nonlinear theories with a good representation of the real vortex flow and satisfying the Kutta-condition at the trailing-edge have been published by R.K. Nangia, G.N. Hancock [22] and C. Rehbach [23].

In the present paper two different nonlinear interference problems will be treated in some detail:

(i) High-aspect-ratio wings in ground proximity for small ground distances.

(ii) Slender wing-body-combinations at incidence.

It will be shown in the first example (i) that a nonlinear dependence of aerodynamic coefficients on the angle of incidence may also occur in the case of attached flow, whereas in the second example (ii) a classical case of separated flow will be investigated. Both problems are solved by means of an adequate representation of the real flow, retaining the essential properties of the flow and neglecting effects of higher order.

The two problems have been investigated by the author, D. Hummel [26], and under his supervision by H. Otto [27].

2. Notations

2.1 Symbols

x,y,z	wing-fixed coordinates, Fig.4
ξ,η,ζ	dimensionless coordinates, equ.(9)
x_R,y_R,z_R	fuselage-fixed coordinates, Fig.9
$b = 2s$	wing span
$c(y)$	local chord
$\bar{\bar{c}}$	mean aerodynamic chord
S	wing area
A	aspect ratio
λ	taper ratio
$R(x_R)$	radius of the fuselage
l	length of the fuselage
N_{25}	quarter-chord point of mean aerodynamic chord
e	distance of point N_{25} from fuselage apex
h	ground distance of point N_{25}
α	angle of incidence
$\alpha_B(x_R)$	local angle of incidence at the fuselage
$\alpha_W(x,y)$	local angle of incidence at the wing
c_L	lift coefficient ($= L/q_\infty S$)
c_M	pitching-moment coefficient ($= M/q_\infty S\bar{\bar{c}}$) with respect to point N_{25}, nose-up positiv
c_{Di}	coefficient of induced drag ($= D_i/q_\infty S$)
$c_l(y)$	local lift coefficient
$c_m(y)$	local pitching-moment coefficient
V_∞	free stream velocity
q_∞	dynamic pressure
u,v,w	perturbation velocities, generated by the real wing, equ.(2)
u_s,w_s	perturbation velocities, generated by the image wing
$k(x',y')$	vorticity distribution
$\gamma(y'),\mu(y')$	spanwise vorticity distributions according to equ.(7)
i,i',i'',i''' j,j',j'',j'''	influence functions. (For details see [26] and [27])

2.2 Subscripts

0	corresponding to zero lift
F,W,R	corresponding to front-part, wing-part and rear-part of a wing-body-combination
v,25,h	corresponding to leading-edge, quarter-chord-line and trailing-edge.

3. High-aspect-ratio wings in close ground proximity

3.1 Experimental results

The lift and pitching-moment curves $c_L(\alpha)$ and $c_L(c_M)$ of a rectangular wing of aspect ratio $A = 2,8$ are plotted in Fig.2 for various ground distances h/c after experiments due to H. John [24]. Results of the linear lifting-surface theory for wings in ground proximity after K. Gersten [13] are also drawn for comparison. At large ground distances, $h/c = \infty$ and $h/c = 1,0$, the experimental data are fairly well predicted by the linear theory. At small ground distance, $h/c = 0,2$, however, the linear theory yields only the slope of the aerodynamic coefficients for small angles of incidence. At larger angles of incidence considerable nonlinear parts of the aerodynamic coefficients occur, especially for the pitching-moment coefficient. Detailed studies have shown, that the flow is completely attached for all ground distances of the wing. Therefore, the nonlinear dependence of the aerodynamic coefficients on the angle of incidence at small ground distances cannot be due to any flow separations, but must be an aerodynamic interference effect in attached flow.

3.2 Theoretical approach

3.2.1 Fundamentals, image principle

The basic equation for the solution of the present interference problem is the equation for the perturbation potential φ in inviscid incompressible flow

$$(1) \qquad \varphi_{xx} + \varphi_{yy} + \varphi_{zz} = 0 \ .$$

From the perturbation potential φ result the perturbation velocities u,v,w as

$$(2) \qquad u = \varphi_x \ , \quad v = \varphi_y \ , \quad w = \varphi_z \ .$$

Ignoring wing thickness the wing is replaced by a lifting-surface vortex-model, which satisfies equ.(1). The unknown vortex strength $k(x',y')$ within the lifting-surface is calculated from the tangent-flow condition at the wing surface, which is the boundary condition of equ.(1). In addition the Kutta-condition of zero load at the wing trailing-edge is fulfilled, which determines the solution completely.

The present problem of a wing in ground proximity is treated by the well-known image principle. The boundary condition of tangential flow at the ground plane is satisfied automatically by adding an image wing and an image vortex system below the ground plane as shown in Fig.3. Thus, the problem of a wing in ground proximity is replaced by the problem of interference between two wings. The aerodynamic forces acting on the real wing under consideration are due to the parallel flow with the velocity V_∞ and due to additional velocities u_s and w_s induced by the image wing. These induced velocities have to be taken into account in the condition of tangent-flow at the surface of the real wing as shown in

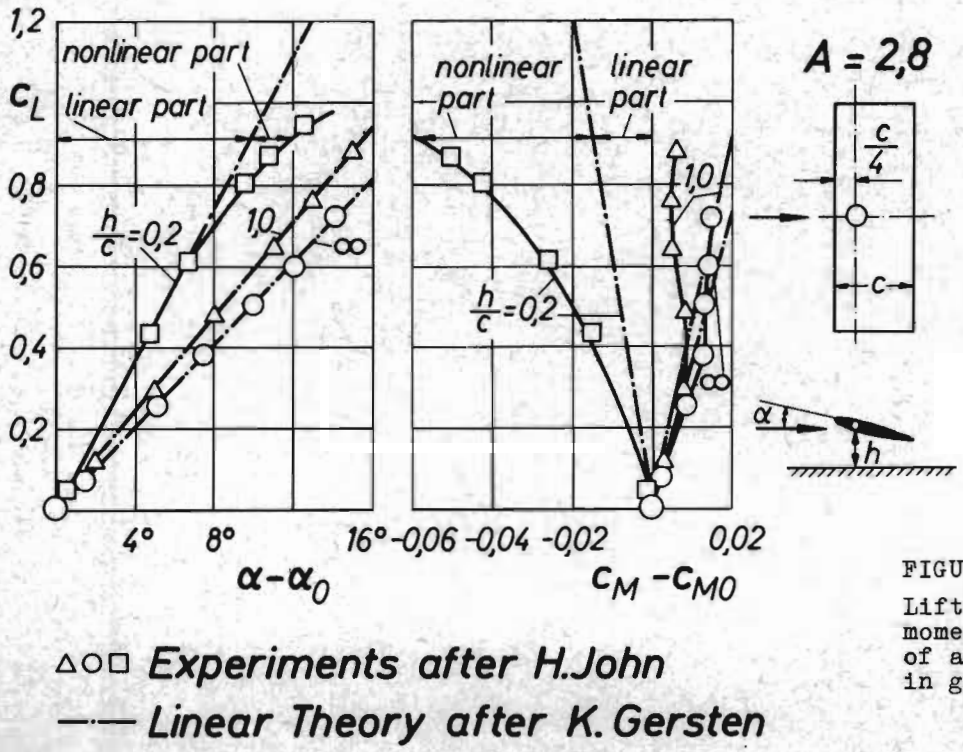

FIGURE 2:
Lift and pitching-moment coefficients of a rectangular wing in ground proximity

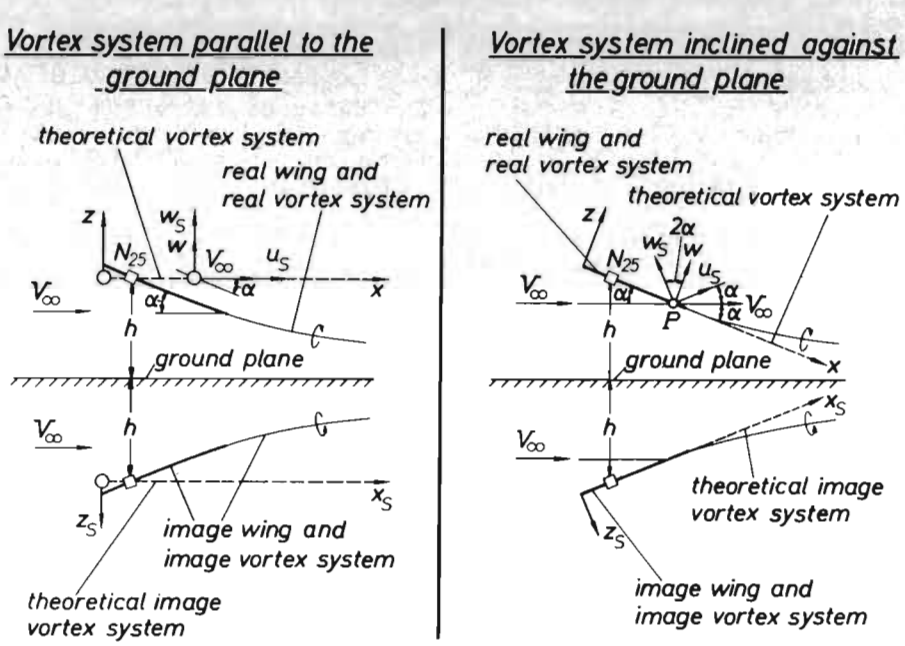

FIGURE 3: Representation of a wing in ground proximity by different vortex models

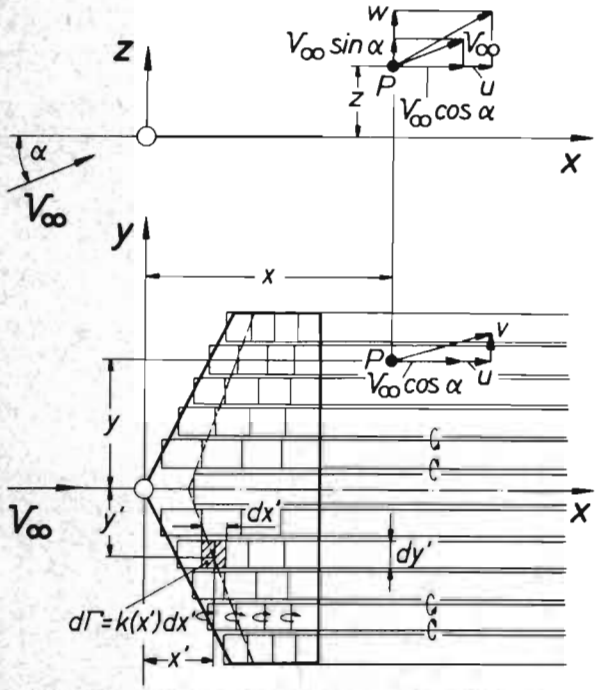

FIGURE 4: Calculation of the induced velocities in the vicinity of a plane vortex system according to lifting-surface theory

Fig.3 as well as in the calculation of the aerodynamic coefficients from the vortex distribution.

3.2.2 Calculation of the induced velocities

As the basis for the solution of the interference problem the induced velocities in the vicinity of a vortex system have to be calculated. This has been done for the plane vortex model of the lifting-surface theory and for a given distribution of vorticity $k(x',y')$ by K. Gersten [25] and D. Hummel [26]. The induced velocities according to Fig.4 are

$$(3)\quad u(x,y,z) = \frac{1}{4\pi} \int_{-s}^{+s} \int_{x_v}^{x_h} k(x',y') \frac{z}{r^3}\, dx'dy'$$

$$(4)\quad v(x,y,z) = -\frac{1}{4\pi} \int_{-s}^{+s} \int_{x_v}^{x_h} k(x',y') \times \left[\frac{2(y-y')z}{[(y-y')^2+z^2]^2} \left(1 + \frac{x-x'}{r}\right) + \frac{(y-y')z}{(y-y')^2+z^2} \frac{x-x'}{r^3} \right] dx'dy'$$

$$(5)\quad w(x,y,z) = \frac{1}{4\pi} \int_{-s}^{+s} \int_{x_v}^{x_h} k(x',y') \left[\frac{(y-y')^2-z^2}{[(y-y')^2+z^2]^2} \left(1 + \frac{x-x'}{r}\right) - \frac{z^2}{(y-y')^2+z^2} \frac{x-x'}{r^3} \right] dx'dy'$$

$$(6)\quad \text{with } r^2 = (x-x')^2 + (y-y')^2 + z^2 \quad .$$

The vorticity distribution $k(x',y')$ may be given according to

$$(7)\quad k(\varphi,\vartheta) = \frac{2}{\pi}\frac{bV_\infty}{\pi c(\vartheta)}\left[\gamma(\vartheta)\cot\frac{\varphi}{2} + 4\mu(\vartheta)\left(\cot\frac{\varphi}{2} - 2\sin\varphi\right)\right]$$

with the relations $\varphi(x',y')$ and $\vartheta(y')$ as

$$(8)\quad \frac{1}{2}(1-\cos\varphi) = \frac{x'-x_v(y')}{c(y')}$$

$$(9a)\text{ and}\quad \cos\vartheta = \frac{y'}{s}\ .$$

Introducing equ.(7) into equ.(3) to (5) and using dimensionless coordinates

$$(9b)\quad \xi = \frac{x}{s};\quad \eta = \frac{y}{s},\quad \eta' = \frac{y'}{s},\quad \zeta = \frac{z}{s},\quad \varrho = \frac{r}{s}$$

the induced velocities can be written in the form

$$(10)\quad \frac{u(\xi,\eta,\zeta)}{V_\infty} = \frac{1}{\pi}\int_{-1}^{+1}(i\gamma+j\mu)\,d\eta'$$

$$\frac{v(\xi,\eta,\zeta)}{V_\infty} = -\frac{1}{\pi}\int_{-1}^{+1}(i'\gamma+j'\mu)\frac{(\eta-\eta')\zeta}{\left[(\eta-\eta')^2+\zeta^2\right]^2}d\eta' -$$

$$(11)\qquad -\frac{1}{\pi}\int_{-1}^{+1}(i''\gamma+j''\mu)\frac{(\eta-\eta')\zeta}{\left[(\eta-\eta')^2+\zeta^2\right]^2}d\eta'$$

$$\frac{w(\xi,\eta,\zeta)}{V_\infty} = \frac{1}{2\pi}\int_{-1}^{+1}(i'\gamma+j'\mu)\frac{(\eta-\eta')^2-\zeta^2}{\left[(\eta-\eta')^2+\zeta^2\right]^2}d\eta' -$$

$$(12)\qquad -\frac{1}{\pi}\int_{-1}^{+1}(i''\gamma+j''\mu)\frac{\zeta^2}{\left[(\eta-\eta')^2+\zeta^2\right]^2}d\eta'.$$

In equ.(10) to (12) i,i',i'' and j,j',j'' are influence functions which are written down and plotted in [26]. These influence functions result from the integration in chordwise direction. They are merely geometrical relations which depend only on the position η' of the inducing wing section and on the location of the sensing point ξ,η,ζ. For points in the plane of the wing $\zeta = 0$ equ.(12) yields

$$(13)\quad \frac{w(\xi,\eta,0)}{V_\infty} = \frac{1}{2\pi}\int_{-1}^{+1}\frac{d}{d\eta'}\left[i'\gamma+j'\mu\right]\frac{d\eta'}{\eta-\eta'}\ .$$

The evaluation of the spanwise integrals in equ.(10) to (12) may be performed by

$$(14)\quad \frac{u(\xi,\eta,\zeta)}{V_\infty} = \sum_{n=1}^{M} c_n(i_n\gamma_n+j_n\mu_n)$$

$$(15)\quad \frac{v(\xi,\eta,\zeta)}{V_\infty} = -\sum_{n=1}^{M} b_n\left[(i_n'+i_n'')\gamma_n+(j_n'+j_n'')\mu_n\right]$$

$$(16)\quad \frac{w(\xi,\eta,\zeta)}{V_\infty} = -\sum_{n=1}^{M}\left[a_n(i_n'\gamma_n+j_n'\mu_n) + d_n(i_n''\gamma_n+j_n''\mu_n)\right]\ .$$

The coefficients within these sums a_n, b_n, c_n and d_n are given by K. Gersten [25] and D. Hummel [26].

The present method for the calculation of the induced velocities in the vicinity of a lifting surface was checked by experiments on a rectangular wing of aspect-ratio $A = 3$. The distribution of local lift and pitching-moment with respect to the wing span

$$(17)\quad c_l = \frac{2b}{c}\gamma \quad\text{and}\quad c_m = \frac{2b}{c}\mu$$

was calculated after the lifting-surface theory of E. Truckenbrodt [3] and the induced velocities according to equ.(14) to (16). The comparison with experimental data given in [26] shows excellent agreement especially in close proximity of the wing. Therefore the method is well suited for the solution of interference problems. It has been applied in the present problem of large-aspect-ratio wings in close proximity to the ground.

3.2.3 Vortex models

The wings in ground proximity have been treated by the image technique as shown in Fig.3. In order to find out the reasons for the nonlinear dependence of the aerodynamic coefficients on the angle of incidence two different vortex models, either parallel to the ground or inclined against the ground, have been used. In both cases the influence of the longitudinal velocity components $u_s(x,y)$, produced by the image wing underneath, has been studied by taking into account these velocities or neglecting them.

3.2.3.1 Vortex system parallel to the ground

The vortex system parallel to the ground which is used in linear theory for small angles of incidence is shown in Fig.3a. The ground distance of the two plane vortex sheets is that of a representative point of the wing such as the quarter-chord-point of mean aerodynamic chord, N_{25}. The position of the two vortex sheets is fixed thus being independent of the angle of incidence. The tangent-flow condition is satisfied on the vortex sheet

$$(18)\quad \alpha = -\frac{w}{V_\infty} - \frac{w_s}{V_\infty} - \frac{u_s}{V_\infty}\cdot\alpha\ .\quad(\alpha\ \text{small})$$

The perturbation velocity w is produced by the vortex system of the real wing, whereas u_s and w_s result from the image wing underneath. Since w, u_s and w_s are linear functions of the angle of incidence α, equ.(18) is actually a nonlinear equation with respect to α. Introducing the induced velocities from equ.(10) and (12) leads to the integral equation

$$\alpha = \frac{1}{2\pi}\int_{-1}^{+1}\frac{d}{d\eta'}\left[i'(\eta;0)\gamma+j'(\eta;0)\mu\right]\frac{d\eta'}{\eta-\eta'} + \frac{1}{2\pi}\int_{-1}^{+1}\left[i'(\eta;\tfrac{2h}{s})\gamma+j'(\eta;\tfrac{2h}{s})\mu\right]\frac{(\eta-\eta')^2-4(h/s)^2}{\left[(\eta-\eta')^2+4(h/s)^2\right]^2}\,d\eta' -$$

$$(19)\quad -\frac{1}{\pi}\int_{-1}^{+1}\left[i''(\eta;\tfrac{2h}{s})\gamma+j''(\eta;\tfrac{2h}{s})\mu\right]\frac{4(h/s)^2}{\left[(\eta-\eta')^2+4(h/s)^2\right]^2}\,d\eta' + \frac{\alpha}{\pi}\int_{-1}^{+1}\left[i(\eta;\tfrac{2h}{s})\gamma+j(\eta;\tfrac{2h}{s})\mu\right]d\eta' .$$

According to the lifting-surface theory after E. Truckenbrodt [3] equ.(19) is satisfied along the quarter-chord-line and along the trailing-edge. Applying equ.(14) and (16), equ.(19) can be transformed into a system of 2M linear equations for 2M unknown values of γ and μ. Equ.(19) has been solved for different values of α with and without taking into account the last nonlinear term.

3.2.3.2 Vortex system inclined against the ground

Another nonlinear effect may be due to the inclination of the wing against the ground. Therefore a plane vortex system inclined against the ground as shown in Fig.3b was used. Since the slope of a vortex sheet far downstream of a wing has no significant effect on the aerodynamic coefficients of the wing, the unrealistic intersection of the two vortex sheets with the ground plane has been conceded. In this case the exact tangent-flow condition is

$$(20)\quad \sin\alpha = -\frac{w}{V_\infty} - \frac{w_s}{V_\infty}\cos 2\alpha - \frac{u_s}{V_\infty}\sin 2\alpha .$$

Since the position of the vortex sheets relative to the ground depends on the angle of incidence, the velocities u_s and w_s, induced by the image vortex system, are nonlinear functions of the angle of incidence. Therefore equ.(20) is nonlinear with respect to α even if the last term is not taken into account. Applying equ.(10) and (12) leads to the integral equation

(21) see below.

ξ_p an ζ_p denote the position of the sensing point on the real wing in a coordinate system fixed to the plane vortex sheet of the image wing. Equ.(21) has been transformed into a system of linear algebraic equations, which has been solved for different values of α.

3.2.4 Aerodynamic coefficients

From the vorticity distribution $k(x,y)$ in the lifting surface the local lift and pitching-moment coefficients result as

$$(22)\quad c_l(y) = 2\int_{x_v}^{x_h}\left[1+\frac{u_s}{V_\infty}\cos\alpha - \frac{w_s}{V_\infty}\sin\alpha\right]\times \times \frac{k(x,y)}{V_\infty}\,\frac{dx}{c(y)}$$

$$(23)\quad c_m(y) = -2\int_{x_v}^{x_h}\left[1+\frac{u_s}{V_\infty}\cos\alpha - \frac{w_s}{V_\infty}\sin\alpha\right]\times \times \frac{x-x_{25}}{c(y)}\,\frac{k(x,y)}{V_\infty}\,\frac{dx}{c(y)} .$$

The evaluation of these two equations was performed by neglecting the last term in square brackets and by replacing $u_s(x,y) \approx u_{s25}(y)$. The integration over the span leads to the overall force and moment coefficients

$$(24)\quad c_L = A\int_{-1}^{+1}(1+\frac{u_{s25}}{V_\infty}\cos\alpha)\gamma(\eta)\,d\eta$$

$$(25)\quad c_{MNose} = -A\int_{-1}^{+1}(1+\frac{u_{s25}}{V_\infty}\cos\alpha)\left[\frac{x_{25}}{\bar{c}}\gamma(\eta) - \frac{c(\eta)}{\bar{c}}\mu(\eta)\right]d\eta$$

$$(26)\quad c_{Di} = -\frac{A}{2}\int_{-1}^{+1}\left[\frac{w(\eta)}{V_\infty}+\frac{w_s(\eta)}{V_\infty}\right]_{x\to\infty}\gamma(\eta)d\eta .$$

The term in square brackets of equ.(26) represents the induced angle of incidence far downstream of the wing. For the inclined vortex model, which intersects the ground behind the wing, $w_s(x\to\infty,\eta)$ was calculated for the ground distance of the trailing-edge.

3.3 Sample calculations and comparison with experimental data

The various theories, developed in this chapter, have been applied to examples for

$$\sin\alpha = \frac{1}{2\pi}\int_{-1}^{+1}\frac{d}{d\eta'}\left[i'(\eta;0)\gamma+j'(\eta;0)\mu\right]\frac{d\eta'}{\eta-\eta'} + \frac{\cos 2\alpha}{2\pi}\int_{-1}^{+1}\left[i'(\xi_p,\zeta_p)\gamma+j'(\xi_p,\zeta_p)\mu\right]\frac{(\eta-\eta')^2-\zeta_p^2}{\left[(\eta-\eta')^2+\zeta_p^2\right]^2}d\eta' -$$

$$(21)\quad -\frac{\cos 2\alpha}{2\pi}\int_{-1}^{+1}\left[i''(\xi_p,\zeta_p)\gamma+j''(\xi_p,\zeta_p)\mu\right]\frac{\zeta_p^2}{\left[(\eta-\eta')^2+\zeta_p^2\right]^2}d\eta' + \frac{\sin 2\alpha}{\pi}\int_{-1}^{+1}\left[i(\xi_p,\zeta_p)\gamma+j(\xi_p,\zeta_p)\mu\right]d\eta' .$$

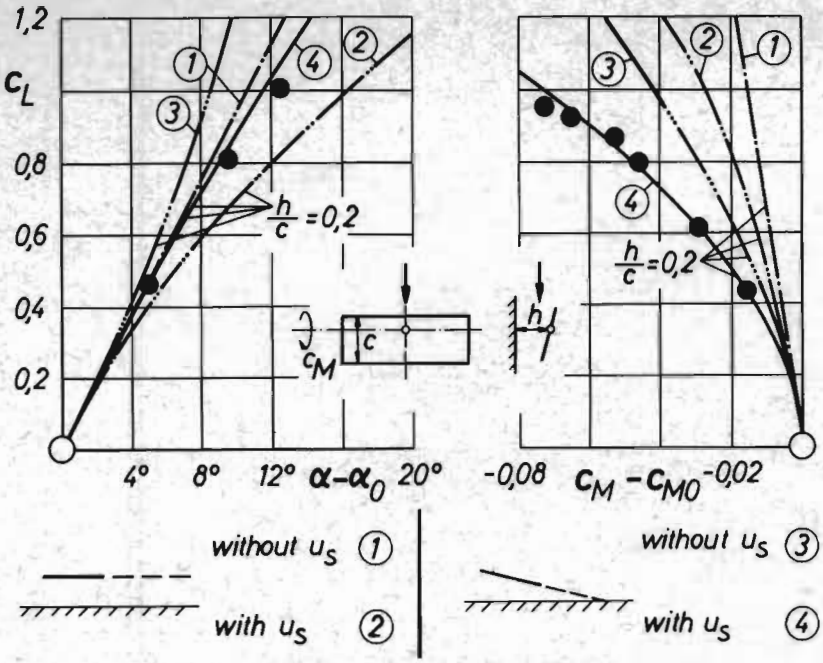

FIGURE 5:
Lift and pitching-moment of a rectangular wing A = 2,8 at ground distance h/c = 0,2. Comparison of different theories with experiments

● *Experiments after H.John*

which experimental data are available. The purpose of these sample calculations was to find out the reasons for the nonlinear dependence of the aerodynamic coefficients on the angle of incidence by comparison with experiments.

Fig.5 shows the experimental lift and pitching-moment coefficients of a rectangular wing of aspect ratio A = 2,8 at ground distance h/c = 0,2 after H.John [24]. In the two diagrams the angle of incidence for zero lift, α_0, and the pitching-moment coefficient for zero lift, c_{M0}, have been subtracted, because for wings in ground proximity these quantities depend on the wing thickness which has been neglected in the theory. The curves ① turn out for the vortex model parallel to the ground and neglecting the u_s-components induced by the image vortex system. This is the well-known linear theory for wings at large ground distances as developed for instance by K. Gersten [13]. Taking into account the u_s-components for the vortex model parallel to the ground, curves ②,

● *Experiments after H.John*

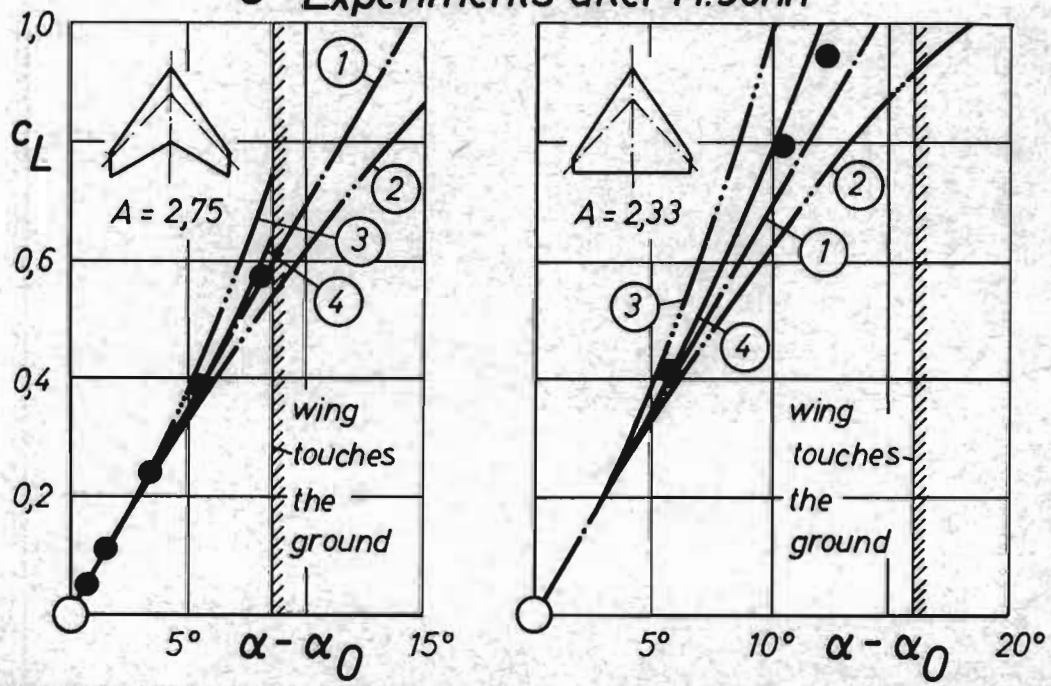

FIGURE 6: Lift coefficients for an A = 2,75 swept wing and an A = 2,33 delta wing at ground distance h/c = 0,2. Comparison of different theories with experiments (Notations see Figure 5)

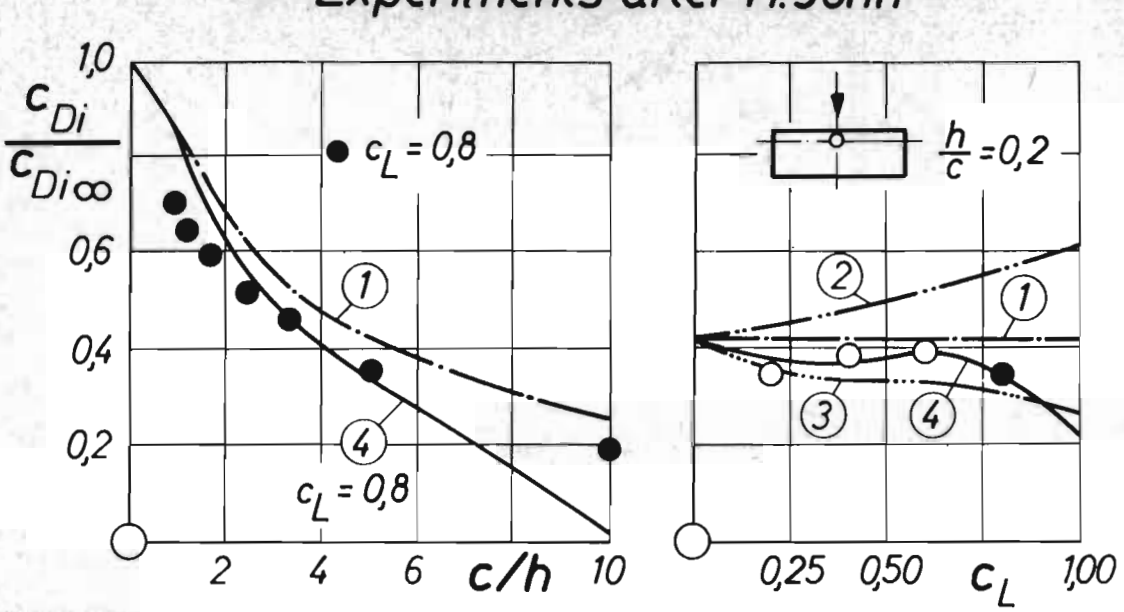

FIGURE 7: Induced drag of a rectangular wing A = 2,8 in ground proximity. Comparison of different theories with experiments (Notations see Figure 5)

the lift is reduced, the nose-down pitching moment is increased, and both coefficients depend nonlinearly on the angle of incidence. If, on the other hand, the inclination of the wing against the ground is considered without taking into account the u_s-components produced by the image vortex system, curves ③, lift and nose-down pitching-moment also depend nonlinearly on the angle of incidence and are increased as compared with curve ①. If both effects, namely the inclination of the wing against the ground and the u_s-components, are taken into account simultaneously, the nonlinear curves ④ result, which are in fairly good agreement with the experimental data. For the lift coefficient, c_L, the two effects cancel each other out to a large amount, thus leading only to a slightly nonlinear lift curve. For the pitching-moment the two effects add up in such a way that a highly nonlinear dependence $c_L(c_M)$ occurs.

Similar results have been obtained for other wing planforms as shown for example in Fig.6 for a 50° sweptback wing of aspect ratio A = 2,75 and for a delta wing of aspect ratio A = 2,33 and taper ratio λ = 0,125, taken from ref. [26]. The nonlinear lifting-surface theory, in which the inclination against the ground as well as the u_s-components induced by the image wing have been taken into account, curves ④, shows fairly good agreement with experimental data. Compared with the corresponding linear theory the nonlinear theory leads to lower values of the lift coefficient for the rectangular wing, Fig. 5, and to slightly larger ones for the swept wing and for the delta wing, Fig.6.

Drag characteristics for the rectangular wing are shown in Fig.7. The induced drag with ground effect divided by the one without ground effect is plotted as a function of ground distance for constant lift coefficient, $c_L = 0,8$, and as a function of lift coefficient for constant ground distance h/c = 0,2. The drag data are not so well predicted as the lift and pitching-moment coefficients. The well-known drag reduction with decreasing ground distance as calculated by the nonlinear theory is in better agreement with the experiments than that after linear theory. For the special ground distance h/c = 0,2 the dependence of the induced drag on the lift coefficient is very well predicted by the nonlinear theory.

3.4 Conclusions

The nonlinear behaviour of large-aspect-ratio wings at small ground distances is found to be the outcome of two nonlinear effects in completely attached flow, which occur simultaneously, namely

(i) the influence of the inclination of the wing against the ground plane and

(ii) the effect of the induced longitudinal perturbation velocities caused by the image wing underneath.

4. Slender wing-body-combinations at incidence.

4.1 Experimental results

The aerodynamic characteristics of slender wing-body-combinations have been investigated in an extensive research program by H. Otto [27]. Three-component wind-tunnel measurements as well as studies of the

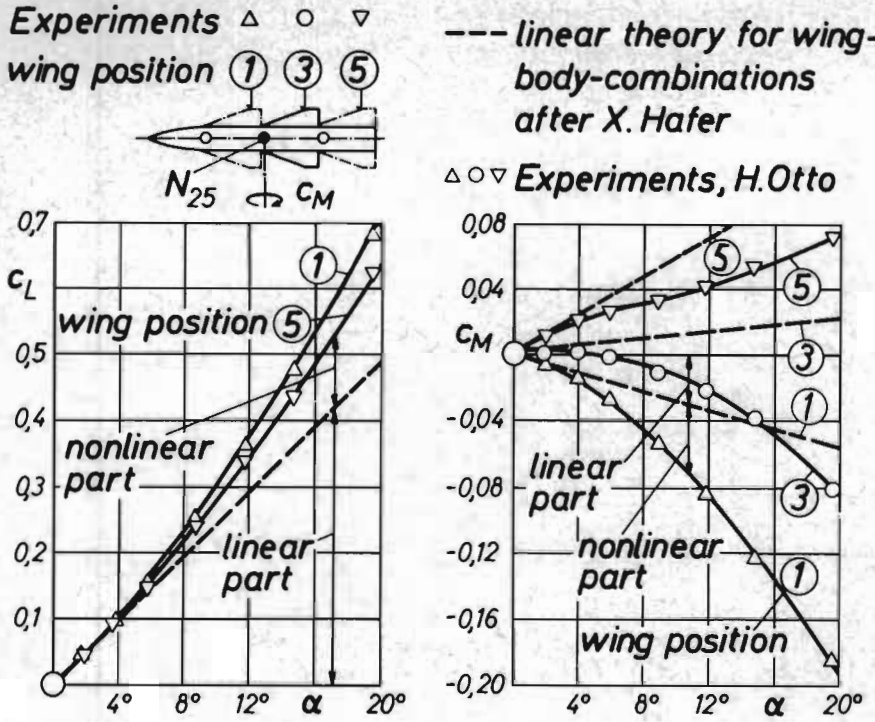

FIGURE 8:
Lift and pitching-moment coefficients of slender wing-body-combinations with different rear positions of the wing

flow in a water-tunnel have been carried out on various slender wings, fuselages and their combinations. Three sharp-edged wings of aspect-ratio $A = 1,0$ and of taper ratios $\lambda = 1,0$ (rectangular wing), $\lambda = 0,5$ (trapezoidal wing) and $\lambda = 0,125$ (cropped delta wing) have been investigated. The five fuselages used in the tests had thickness/length ratios of 0,05 and 0,10 and were cylindrical bodies with various shapes of the nose and the afterbody. The wing-body-combinations had body-thickness/wing-span ratios of 0,2 and 0,4. The wings were located at the fuselage center-line and their rear position was altered in a wide range.

The lift and pitching-moment curves $c_L(\alpha)$ and $c_M(\alpha)$ for combinations of a cylindrical fuselage having an ogival nose and the $A = 1,0$ cropped delta wing are plotted in Fig.8 for various rear positions of the wing relative to the fuselage [27]. The results of the linear theory for wing-body-combinations after X. Hafer [10] are also drawn for comparison. The aerodynamic coefficients depend nonlinearly on the angle of incidence and the linear theory yields only the slope of the aerodynamic coefficients for small angles of incidence.

Visualization of the flow in the water-tunnel has shown that even at small angles of incidence the flow separates from the leading edges of the wing and from the fuselage as illustrated in Fig.1. Therefore, the occurrence of a nonlinear dependence of the aerodynamic coefficients on the angle of incidence is -at least for the most part- due to flow separations as it is well-known for slender sharp-edged wings and slender bodies. On the other hand, Fig.8 shows that the nonlinear parts of the aerodynamic coefficients depend on the position of the wing with respect to the fuselage. (The different linear parts of the pitching-moment coefficients are due to the choice of a wing-fixed pitching-moment reference point, N_{25}). The nonlinear part of the aerodynamic coefficients decreases with increasing distance of the wing from the apex of the fuselage. From this may be concluded, that interference effects between wing and fuselage also contribute to the nonlinear dependence of the aerodynamic coefficients on the angle of incidence.

For combinations of slender wings and fuselages with vortex type flow separations at the wing and at the fuselage, the occurrence of nonlinear aerodynamic coefficients may be due to the following facts:

(i) the effect of the trailing vortices of the wing on the wing itself,

(ii) an interference effect of the wing vortices on the fuselage

(iii) the effect of the trailing vortices of the fuselage on the fuselage itself and

(iv) an interference effect of the fuselage vortices on the wing.

Detailed studies of the flow, performed by H. Otto [27], have shown, that on slender wing-body-combinations having a body-thickness/wing-span ratio smaller than 0,4 the vortices resulting from the flow separations at the fuselage are much weaker than the vortices according to the flow separations at the wing. Therefore, the effects of the fuselage vortices, (iii) and (iv), are small as compared with those of the wing vortices, (i) and (ii). In addition to the well-known effect of the wing vortices on the wing itself, (i), for wing-

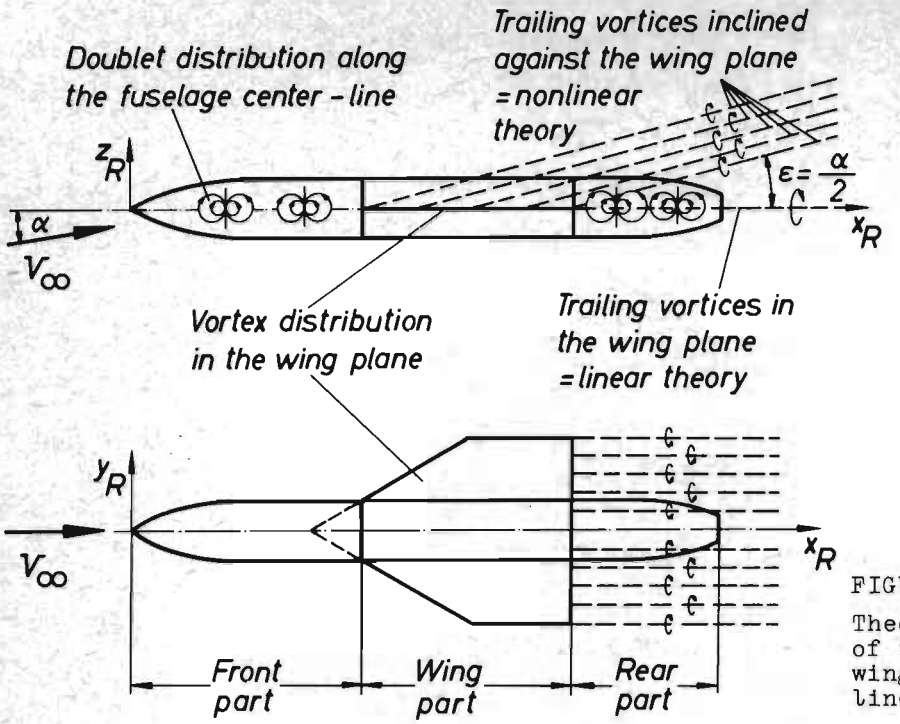

FIGURE 9:
Theoretical representation of the flow around a slender wing-body-combination in linear and nonlinear theory

body-combinations an interference effect turned out to be also important, which mainly results from the influence of the wing vortices on that part of the fuselage which is located behind the wing, (ii).If, therefore, the rear position of the wing with respect to the fuselage is increased, this interference effect decreases and the nonlinear parts of the lift coefficient and especially of the pitching-moment coefficient are reduced.

4.2 Theoretical approach

4.2.1 Theoretical representation of the flow

Considering the experimental results, mentioned above, the linear theory of lifting wing-body-combinations after X. Hafer [10] has been extended by H. Otto [27] to the calculation of nonlinear lift and pitching-moment coefficients of slender wing-body-combinations. The fairly weak trailing vortices of the fuselage have been neglected in these calculations and only the effects of the trailing vortices of the wing have been taken into account.

In the linear theory of X. Hafer [10] the wing-body-combination is divided into three parts as shown in Fig.9, namely the front and rear part of the fuselage upstream and downstream of the wing, respectively, and the wing part of the combination which comprises the wing and the corresponding part of the fuselage. In the theory the fuselage is represented by a center-line distribution of doublets, which is nonzero in the front and in the rear part of the fuselage and which is zero in the wing part of the fuselage because of the velocities induced there by the wing. In the linear theory of X. Hafer [10] the wing is replaced by a continuous distribution of vortices and a trailing vortex sheet which is located in the plane of the wing as indicated in Fig.9. In the nonlinear theory of H. Otto [27] the wing part of the combination is represented by the vortex model of the nonlinear lifting-surface theory after K. Gersten [17], which is also marked in Fig.9. In this theory the trailing vortices are located in plane sheets inclined at an angle of $\varepsilon = \alpha/2$ with respect to the wing plane. For this vortex model of the flow the effect of the trailing vortices on the wing itself, (i), can be calculated by means of the nonlinear theory of K. Gersten [17].

4.2.2 Calculation of the induced velocities

In order to determine the interference effect of the trailing wing-vortices on the fuselage, (ii), the induced velocities produced by the system of trailing vortices inclined at the angle $\varepsilon = \alpha/2$ have to be calculated at the fuselage center-line. Fig.10 shows one plane vortex sheet out of the whole trailing vortex system. The induced upwash normal to the vortex sheet d^2w_n in an arbitrarily located point $P(x,y,z)$, generated by a horse-shoe vortex of strength $k(x',y')dx'$ and span dy' located at x',y' is

$$d^2w_n = \left\{ \frac{(y-y')^2 - [z\cos\varepsilon - (x-x')\sin\varepsilon]^2}{\left\{(y-y')^2 + [z\cos\varepsilon - (x-x')\sin\varepsilon]^2\right\}^2} \times \right.$$

$$(27) \quad \times \left[1 + \frac{(x-x')\cos\varepsilon + z\sin\varepsilon}{r} \right] -$$

$$- \frac{[z\cos\varepsilon - (x-x')\sin\varepsilon]^2}{(y-y')^2 + [z\cos\varepsilon - (x-x')\sin\varepsilon]^2} \times$$

$$\left. \times \frac{(x-x')\cos\varepsilon + z\sin\varepsilon}{r^3} \right\} \frac{k(x',y')}{4\pi}\, dx'dy'$$

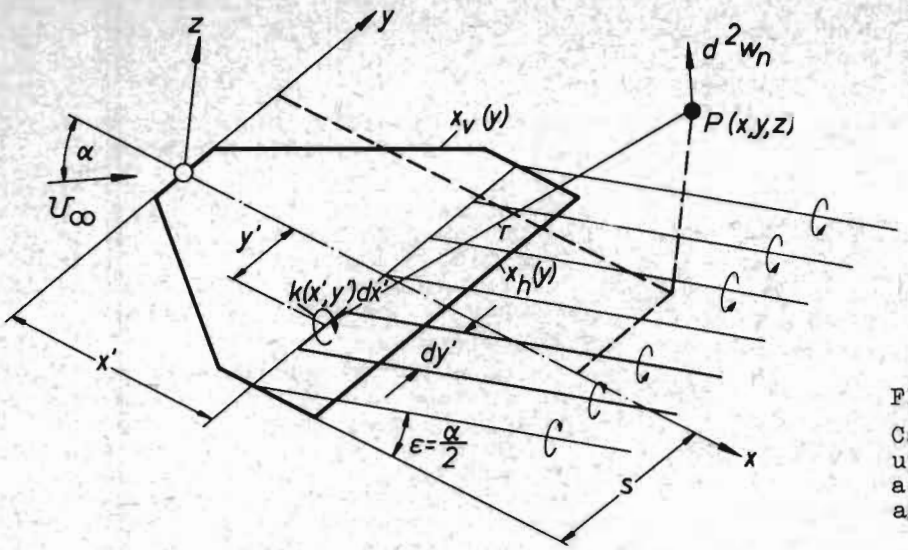

FIGURE 10:
Calculation of the induced upwash in the vicinity of a vortex system inclined against the wing plane

with r according to equ.(6). For points on the fuselage center-line, y=z=0, the induced upwash results for small angles of incidence as

$$w(x,\varepsilon)=\frac{1}{4\pi}\int_{-s}^{+s}\int_{x_v}^{x_h} k(x',y')\left\{\frac{y'^2-(x-x')^2\sin^2\varepsilon}{y'^2+(x-x')^2\sin^2\varepsilon}\times\right.$$

$$(28)\quad \times\left[1+\frac{(x-x')\cos\varepsilon}{r}\right]-\frac{(x-x')^2\sin^2\varepsilon}{y'^2+(x-x')^2\sin^2\varepsilon}\times$$

$$\left.\times\frac{(x-x')\cos\varepsilon}{r^3}\right\}dx'dy'.$$

Introducing k according to equ.(7) and using the notations of equ.(8) and (9) the induced upwash at the fuselage center-line may be written in the form

$$(29)\quad \frac{w(x,\varepsilon)}{V_\infty}=\frac{1}{4\pi}\int_{-1}^{+1}(i'''\gamma+j'''\mu)d\eta'\ .$$

In this equation i"' and j"' are influence functions as introduced by H. Otto [27], which depend on the position of the inducing wing section η' and on the angle $\varepsilon=\alpha/2$. The evaluation of equ.(29) has been performed by numerical integration.

The induced velocities at the wing produced by the doublet distribution of the fuselage have also to be considered. The wing part of the wing-body-combination is replaced by a flat wing in the plane z=0. The upwash at the wing outside of the fuselage can be calculated according to X. Hafer [10] as

$$(30)\quad \frac{w(x_R,y_R,0)}{V_\infty}=\frac{1}{2}\int_{x_{R1}}^{x_{R2}}\frac{\alpha_B(x'_R)R_1^2(x'_R)}{\sqrt{(x_R-x'_R)^2+y_R^2}^3}\,dx'_R \qquad |y_R|>R_1.$$

For the region within the fuselage the induced upwash w is calculated according to X. Hafer [10] for the corresponding points at the surface of the fuselage, $x_R,y_R,z_R\neq 0$, and this upwash is assumed to act in the wing plane, $z=z_R=0$. This leads to

$$\frac{w(x_R,y_R)}{V_\infty}=\frac{1}{2}\int_{x_{R1}}^{x_{R2}}\frac{\alpha_B(x'_R)R_1^2(x'_R)\,dx'_R}{\sqrt{(x_R-x'_R)^2+y_R^2+z_R^2}^3}-$$

$$(31)\quad -\frac{3}{2}z_R^2\int_{x_{R1}}^{x_{R2}}\frac{\alpha_B(x'_R)R_1^2(x'_R)\,dx'_R}{\sqrt{(x_R-x'_R)^2+y_R^2+z_R^2}^5} \qquad |y_R|<R_1.$$

In equ.(30) and (31) x_{R1} and x_{R2} denote the boundaries of the doublet distributions on the fuselage center-line and $\alpha_B(x'_R)$ is the distribution of the local angle of incidence along the axis of the fuselage. The two equations have been evaluated for the front part and for the rear part of the wing-body-combination by numerical integration.

4.2.3 Iteration method and aerodynamic coefficients

The calculation of the aerodynamic coefficients of a slender wing-body-combination after the nonlinear theory of H. Otto [27] is performed by the following iteration procedure.

Preliminaries: According to X. Hafer [10] the boundary layer of the fuselage is taken into account by a boundary-layer calculation at the fuselage in axial flow for given Reynolds number after Truckenbrodt's integral method. The resulting displacement-thickness $\delta_1(x_R)$ is added to the given fuselage contour $R(x_R)$ in order to determine the theoretical contour $R_1(x_R)=R(x_R)+\delta_1(x_R)$. The wing-body-combination is then divided into three parts as shown in Fig.9. For each angle of incidence α the following calculations have to be performed.

Iteration procedure

a) The vortex distributions $\gamma(\eta)$ and $\mu(\eta)$ of equ.(7) are calculated by the non-

linear lifting-surface theory after K. Gersten [17] for the wing part of the combination which is assumed to be a flat wing at a given angle of incidence $\alpha_W = \alpha$. A first approximation for the lift c_{LW} and the pitching-moment c_{MW} of the wing part turns out.

b) The distribution of the induced angle of incidence at the fuselage center-line, $\Delta\alpha_B(x_R)$, produced by the wing is then calculated from equ.(29). The contributions of the front part and of the rear part of the wing-body-combination to the aerodynamic coefficients are then calculated for a fuselage at a distribution of local angle of incidence $\alpha_B(x_R) = \alpha + \Delta\alpha_B(x_R)$ according to slender body theory, see [10], as

$$(c_L)_{F,R} = \frac{2\pi}{S} \int_{x_{R1}}^{x_{R2}} \frac{R}{R_1} \frac{d}{dx_R}\left[\alpha_B(x_R) R_1^2(x_R)\right] dx_R \tag{32}$$

and

$$(c_M)_{F,R} = -\frac{2\pi}{S\bar{c}} \int_{x_{R1}}^{x_{R2}} \frac{R(x_R)}{R_1(x_R)} (x_R - e) \times \tag{33}$$

$$\times \frac{d}{dx_R}\left[\alpha_B(x_R) R_1^2(x_R)\right] dx_R \ .$$

The indices F,R denote the front part and the rear part of the combination, x_{R1} and x_{R2} are their boundaries and e is the distance of the pitching-moment reference point form the apex of the fuselage.

c) The addition of the contributions of all three parts of the wing-body-combination according to

$$c_L = c_{LF} + c_{LW} + c_{LR}$$
$$c_M = c_{MF} + c_{MW} + c_{MR} \tag{34}$$

leads to the first approximation of the overall aerodynamic coefficients.

d) The distribution of the induced angle of incidence at the wing, $\Delta\alpha_W(x,y)$, produced by the fuselage is then calculated from equ.(30) and (31). This leads to a distribution of the local angle of incidence at the wing $\alpha_W(x,y) = \alpha + \Delta\alpha_W(x,y)$.

e) The calculation for the wing part of the combination according to a) is performed for the distribution of local angle of incidence $\alpha_W(x,y)$. The calculation process a) to c) and if necessary d) is repeated until the alterations of the overall aerodynamic coefficients are smaller than a certain limit, $|c_{L,i} - c_{L,i-1}| < 0{,}001$ for instance.

The iteration process turned out to be stable and only about three cycles were necessary to calculate the final results.

4.3 Sample calculations and comparison with experimental data

The nonlinear theory of H. Otto [27] has been applied to a large number of wing-body-combinations for which experimental data were available. A typical result is shown in Fig.11. The lift and pitching-moment coefficients $c_L(\alpha)$ and $c_M(\alpha)$ for combinations of an $A = 1{,}0$ cropped delta wing and a cylindrical fuselage having an ogival nose are given for various rear positions of the wing with respect to the fuselage. The linear theory of X. Hafer [10] and the nonlinear theory of H. Otto

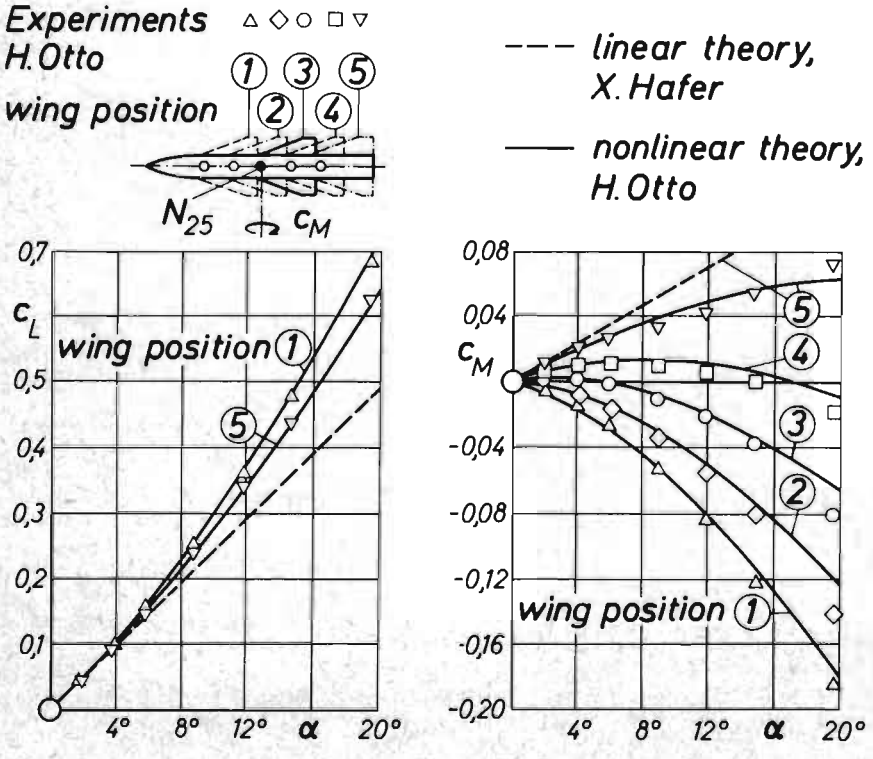

FIGURE 11:
Lift and pitching-moment of slender wing-body-combinations with different rear positions of the wing. Comparison of theory with experiments.

[27] are compared with experimental data [27] . The solid lines are the results of the nonlinear theory of H. Otto [27] and the symbols denote the experimental data. The lift coefficients are shown for two rear positions of the wing, whereas the pitching-moment coefficients are given for five rear positions of the wing. The influence of the wing position on the nonlinear part of the aerodynamic coefficients is the same in the nonlinear theory and in the experimental results and the experimental data are fairly well predicted by the nonlinear theory of H. Otto [27].

Some details of the mechanism of interference are shown in Fig.12. In theory and experiment the aerodynamic coefficients can be split up into a linear part and a nonlinear part according to Fig. 1 as

$$c_L = \left(\frac{dc_L}{d\alpha}\right)_0 \alpha + \Delta c_L$$

$$c_M = \left(\frac{dc_M}{d\alpha}\right)_0 \alpha + \Delta c_M \quad . \tag{35}$$

The nonlinear parts Δc_L and Δc_M consist of contributions from the front part (F), the wing part (W) and the rear part (R) of the wing-body-combination

$$\Delta c_L = \Delta c_{LF} + \Delta c_{LW} + \Delta c_{LR}$$

$$\Delta c_M = \Delta c_{MF} + \Delta c_{MW} + \Delta c_{MR} \quad . \tag{36}$$

Fig. 12 shows these different contributions to the nonlinear parts of the aerodynamic coefficients for combinations of a fuselage having ogival nose and cylindrical afterbody with three wings of aspect ratio A = 1,0 and different planforms located at the same rear position. In all cases the contribution of the front part of the combination to the nonlinear parts of the aerodynamic coefficients is negligibly small and is therefore not shown in Fig.12. Considerable portions of the nonlinear parts of the aerodynamic coefficients result from the wing. The well-known effects of the wing planform on the magnitude of the nonlinear aerodynamic coefficients are also observed in the present interference problem, for which the local angle of incidence at the wing is $\alpha_W(x,y)$ rather than a constant α. The second contribution to the nonlinear parts of the aerodynamic coefficients results from the rear part of the combination. This portion is very important for wing-body-combinations the fuselage of which extends far downstream of the wing trailing-edge. The induced upwash at the fuselage center-line is about the same for all wing-planforms. Therefore, no planform effects are observed for this second contribution to the nonlinear aerodynamic coefficients.

Fig.13 shows a comparison between experimental data and the linear and nonlinear theory for wing-body-combinations with the A = 1,0 cropped delta wing in fixed position relative to the fuselage and two fuselages of different thickness/length ratios, 0,05 and 0,10. These fuselages consisted of a cylindrical central part with elliptical nose and afterbody. The experimental data are fairly well predicted by the nonlinear theory of H. Otto [27] for these configurations, too. The original paper of H. Otto [27] contains much more examples and comparisons between the nonlinear theory and experiments. It turns out that this theory is in good agreement with experiments for slender wing-body-combinations with different wings, various shapes and thickness/length ratios of the fuselages, and for different rear positions of

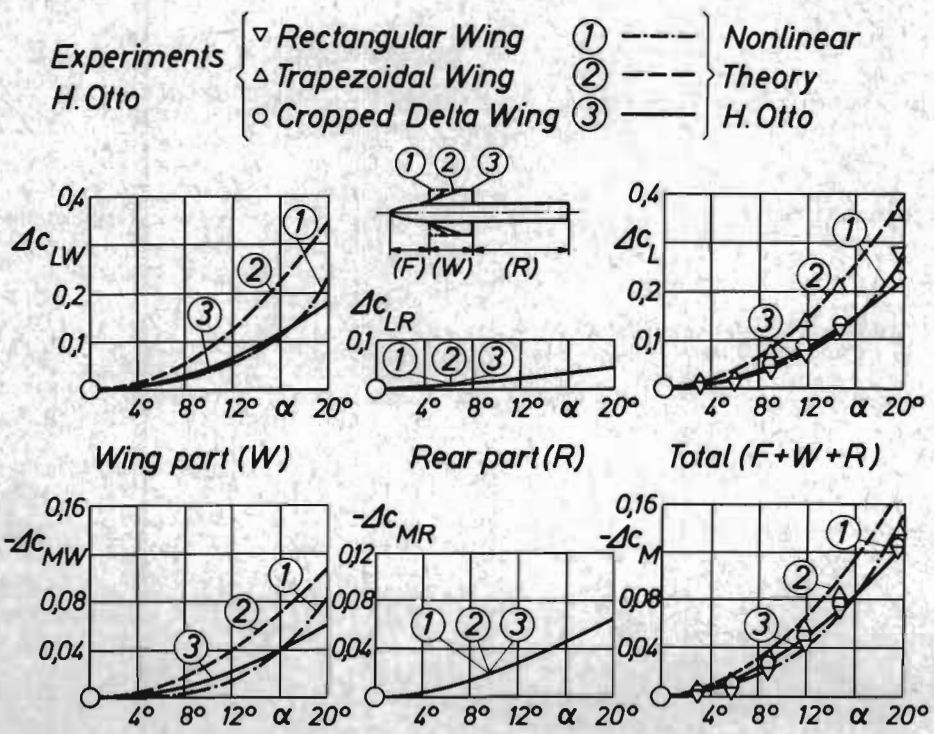

FIGURE 12:
Contributions of wing and rear part of slender wing-body-combinations to the nonlinear parts of the aerodynamic coefficients

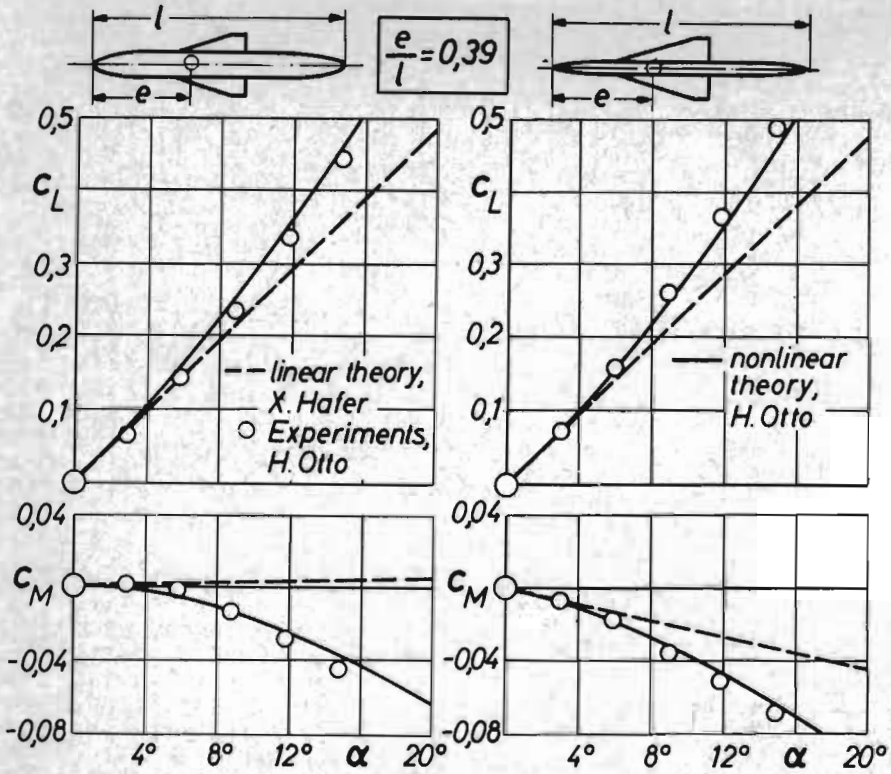

FIGURE 13:
Lift and pitching-moment of slender wing-body-combinations with different fuselages. Comparison of theory with experiment.

the wing relative to the fuselage. From this can be concluded that the nonlinear theory of H. Otto [27] takes into account the essential properties of the physical flow and that only second order effects have been neglected.

4.4 Conclusions

The investigations on slender wing-body-combinations have shown that the nonlinear parts of the aerodynamic coefficients result from

(i) the effect of the trailing vortices of the wing on the wing itself and from

(ii) the interference effect of the trailing vortices of the wing on the fuselage.

As far as the body-thickness/wing-span ratio is smaller than about 0,5 the effects of the fuselage vortices are negligibly small.

5. Final remarks

In the present investigation two fundamentally different interference problems have been dealt with in some detail. The example of a large-aspect-ratio wing in close ground proximity shows, that a nonlinear dependence of the aerodynamic coefficients on the angle of incidence can also occur in completely attached flow. The slender wing-body-combination at incidence on the other hand is a classical problem of separated flow.

Both problems have been solved in such a way that based on experimental studies the theoretical representation of the flow was chosen as simple as possible but as comprehensive as necessary in order to retain the essential properties of the physical flow and to neglect only higher order effects.

For both problems the present approach may be regarded as a first step because only the overall aerodynamic coefficients have been calculated and compared with experimental data. The good agreement, however, indicates that the essential properties of the flow have been taken into account. To calculate the pressure distribution in a second step, much more details of the physical flow would have to be taken into consideration.

6. References

[1] L. Prandtl: Tragflügeltheorie, I. u. II. Mitteilung. Nachrichten der Kgl.Ges.Wiss. Göttingen, Math.-Phys. Klasse 1918, p. 451-477 und 1919, p. 101-137. Wiederabgedruckt in: Gesammelte Abhandlungen, Bd. I, p. 322-372, Springer Verlag Berlin/Göttingen/Heidelberg 1961.

[2] H. Multhopp: Methods for calculating the lift distribution of wings. (Subsonic lifting-surface theory). ARC Rep. Mem. 2884 (1955).

[3] E. Truckenbrodt: Tragflächentheorie bei inkompressibler Strömung. Jahrbuch 1953 der Wiss.Ges.f. Luftfahrt (WGL), p. 40-65.

[4] J.L.Hess, A.M.O.Smith: Calculation of potential flow about arbitrary bodies. Progr. in Aeron. Sci. 8 (1967), p. 1-138.

[5] P.E. Rubbert, G.R. Saaris: A general three-dimensional potential-flow method applied to V/STOL aerodynamics. SAE Paper 68 0304 (1968).

[6] F.A. Woodward: Analysis and design of wing-body-combinations at subsonic and supersonic speeds. J. Aircraft 5 (1968), p. 528-534.

[7] R.L. Carmichael: Recent experience in using finite element methods for the solution of problems in aerodynamic interference. In: Aerodynamic Interference. AGARD-CP-71 (1971), Nr. 4.

[8] Th.E.Labrujere, W.Loeve,J.W.Slooff: An approximate method for the calculation of the pressure distribution on wing-body-combinations at subcritical speeds. In: Aerodynamic Interference. AGARD-CP-71 (1971), Nr. 11.

[9] W. Kraus, P. Sacher: Das Panelverfahren zur Berechnung der Druckverteilung von Flugkörpern im Unterschallbereich. Z.Flugwiss. 21 (1973), p. 301-311.

[10] X. Hafer: Untersuchungen zur Aerodynamik der Flügel-Rumpf-Anordnungen. Jahrbuch 1957 der Wiss. Ges.f.Luftfahrt (WGL), p. 191-207.

[11] F. Thomas: Aerodynamische Eigenschaften von Pfeil- und Deltaflügeln in Bodennähe. Jahrbuch 1958 der Wiss.Ges.f.Luftfahrt (WGL), p. 53-61.

[12] U. Ackermann: Ein Doppeltraglinienverfahren zur Untersuchung des Flügels in Bodennähe. Jahrbuch 1962 der Wiss.Ges.f.Luft-u.Raumfahrt (WGLR), p. 104-109.

[13] K. Gersten: Berechnung der aerodynamischen Beiwerte von Tragflügeln endlicher Spannweite in Bodennähe. Abhandlg.d.Braunschw. Wiss.Ges. 12 (1960),p. 95-115.

[14] G.H. Saunders: Aerodynamic characteristics of wings in ground proximity. Can.Aeron.Space J. 11 (1965), p. 185-192.

[15] U. Ackermann: Zur Berechnung der aerodynamischen Beiwerte und des Strömungsfeldes von Tragflügeln in Bodennähe unter Berücksichtigung von Nichtlinearitäten. Dissertation T.H. Darmstadt 1966.

[16] C.H. Fox: Prediction of lift and drag for slender sharp-edged delta wings in ground proximity. NASA TN D-4891 (1969).

[17] K. Gersten: Nichtlineare Tragflächentheorie, insbesondere für Tragflügel mit kleinem Seitenverhältnis. Habilitationsschrift T.H. Braunschweig 1960. Ing.Archiv 30 (1961), p. 431-452.

[18] C.E. Brown, W.H. Michael: Effect of leading-edge separation on the lift of a delta wing. J.Aero.Sci. 21 (1954), p. 690-694.

[19] K.W. Mangler, J.H.B. Smith: A theory of the flow past a slender delta wing with leading-edge separation. Proc. Roy. Soc. London (A) 251 (1959), p. 200-217.

[20] J.H.B. Smith: Improved calculations of leading-edge separation from slender delta wings. RAE TR 66070 (1966).

[21] E.S.Levinsky, M.H.Y.Wei: Nonlinear lift and pressure distribution on slender conical bodies with strakes at low speeds. NASA CR-1202 (1968).

[22] R.K.Nangia, G.N.Hancock: A theoretical investigation for delta wings with leading edge separation at low speeds. Queen Mary Coll., Univ. of London, Report ARC 30 608 (1968).

[23] C. Rehbach: Calcul d'écoulements autour d'ailes sans épaisseur avec nappes tourbillonnaires évolutives. La Rech.Aérospatiale 1973,p. 53-61.

[24] H. John: Systematische Sechskomponenten-Windkanalmessungen an schiebenden Flügeln in Bodennähe.
Teil I : Rechteckflügel (1964)
Teil II : Pfeilflügel (1965)
Teil III: Deltaflügel (1965)
Berichte des Inst.f.Flugtechnik, T.H. Darmstadt.

[25] K. Gersten: Ueber die Berechnung des induzierten Geschwindigkeitsfeldes von Tragflügeln. Dissertation Braunschweig 1957.Jahrbuch 1957 d.Wiss. Ges.f.Luftfahrt (WGL), p. 172-190.

[26] D. Hummel: Nichtlineare Tragflügeltheorie in Bodennähe.Habilitationsschrift TU Braunschweig 1971. Z. Flugwiss. 21 (1973), 426-442.

[27] H. Otto: Ein Beitrag zu den nichtlinearen Auftriebs- und Nickmomenteneigenschaften von schlanken Flügel-Rumpf-Kombinationen. Dissertation Braunschweig 1972.Deutsche Luft- u. Raumfahrt (DLR),Forschungsbericht (FB) 73-66(1973) and Z. Flugwiss. 22 (1974), No. 5